Synthesis, sintering by Cool-SPS and characterization of A2Cu(CO3)2 (A = K, Na): evidence for multiferroic and magnetoelectric cupricarbonates

Thomas Herisson de Beauvoir, Anna Sangregorio, Iñaki Cornu, Michaël Josse

ARTICLE

Synthesis, sintering by Cool-SPS (Spark Plasma Sintering) and characterization of $A_2Cu(CO_3)_2$ (A = K, Na): evidences for multiferroic and magnetoelectric cupricarbonates

Received 00th January 20xx,
Accepted 00th January 20xx

DOI: 10.1039/x0xx00000x

Thomas Herisson de Beauvoir, Anna Sangregorio, Iñaki Cornu, Michaël Josse

We report here the synthesis and densification of two magnetic materials in the system $A_2Cu(CO_3)_2$ (A = Na, K). Based on literature data, the synthesis route has been modified to offer the possibility of gram-scale production with high powder purity. The Cool Spark Plasma Sintering method has been used to obtain highly dense samples (> 95% of theoretical density). Not only the sintering method proved its efficiency on getting dense ceramics, but it also extended the stability domain of both compounds to higher temperatures. The case of $Na_2Cu(CO_3)_2$ is highly instructive of the possibilities offered by the Cool-SPS technique, since the pure phase can be obtained during sintering process, while it is impossible through conventional heat treatments in a furnace. Obtaining dense ceramics allowed the exploration of dielectric properties, leading to the observation of a step-like anomaly in $K_2Cu(CO_3)_2$ similar to some multiferroic systems, while $Na_2Cu(CO_3)_2$ exhibits an interesting magnetocapacitance evolution, probably linked to a magnetoelectric coupling.

Introduction

Huge efforts were put in the last few years into low temperature processing, and more particularly into low temperature sintering [1–3]. Important developments were made and more understanding of mechanisms is coming out from the large span of materials explored [3–6]. Not only low temperature sintering of ceramics, such as Room Temperature Sintering [7], Cold Sintering Process [2], Hydrothermal Sintering [1] and Cool-SPS (Cool Spark Plasma Sintering) [3], allows time and energy saving. It also widens the opportunities offered by the processing temperatures used. Thus, it is possible to densify ceramic-polymer composites [8,9], control grain growth anisotropy [8] or sinter ceramics with base metals without oxidation nor diffusion at interfaces [10]. Another possibility consists in using sintering as a prospection tool to explore materials whose bulk properties were not characterized so far, due to the impossibility to obtain them as dense samples [3,11–13]. Thermodynamically fragile materials represent a wide range of materials which decomposition/transition temperatures forbid high temperature sintering without modification of their composition/structure [3,13]. Considering now the new possibilities offered by low temperature processing techniques, we focused on candidate (multi)ferroic and magnetoelectric materials showing limited temperature stability. The Cool Spark Plasma Sintering (Cool-SPS) was developed by utilizing SPS apparatus at high pressure, low temperature to stabilize and densify materials with low decomposition temperatures. Its use allows the densification of materials above their decomposition temperature. The involvement of water during sintering seems to enhance densification in some cases [11], but some materials can be densified although dehydrated [12]. Materials such as phosphates [12], sulfates [11], carbonates [3] but also molecular materials [14] can be successfully stabilized and sintered. They represent good candidates since their decomposition occurs before natural sintering is thermally activated. As we already highlighted in a previous work [11], some of these materials show interesting properties such as multiferroicity and magnetoelectric couplings. However, their sintering mechanisms remains different and more complex than conventional sintering pathways [11,12] and require specific investigations. Efforts are made to understand low temperature sintering mechanisms [15–17] to determine their advantages, weaknesses and complementarities. While many examples of oxides are proposed in literature [18–21], fewer examples of non-oxide phases exist. Here we focus on two carbonates of composition $A_2Cu(CO_3)_2$ (A = Na, K), known for their magnetic properties [22,23], facing decomposition at temperatures below 300 °C. First, we present an adapted synthesis route allowing the preparation of pure powders at the gram scale, which is a prerequisite for sintering experiments. Then, we show the effect of sintering on both powders and compare their behaviour, in regard with their decomposition temperature. We eventually highlight their bulk electrical and magnetoelectric behaviour.

Experimental section

[a] *Address here.*
[b] *Address here.*
[c] *Address here.*
† Footnotes relating to the title and/or authors should appear here.
Electronic Supplementary Information (ESI) available: [details of any supplementary information available should be included here]. See DOI: 10.1039/x0xx00000x

Synthesis of $K_2Cu(CO_3)_2$ (noted KCCO in the following) powder have been adapted from methods proposed by Deville, Pickering and Applebey on various copper carbonate systems [24–27]. The case of $Na_2Cu(CO_3)_2$ (noted NaCCO) is slightly different since the direct synthesis of phase pure powder of the anhydrous form is impossible using the processes reported in the literature. Chalconatronite [28], a tri-hydrated form ($(Na_2Cu(CO_3)_2{\cdot}3H_2O$, noted hyd-NaCCO in the following) must be prepared first and inserted for 24h in a boiling aqueous sodium carbonate-bicarbonate solution. Small crystals of anhydrous $Na_2Cu(CO_3)_2$ form, which must be separated from an unidentified phase forming during the process [29]. In the present work, in order to produce powder quantities large enough to achieve sintering experiments, this process appears unsuitable. We recently proposed a sintering method using SPS technique and an hydrated precursor, which is subsequently dehydrated during sintering process [11], and this method has been successfully applied to $Na_2Cu(CO_3)_2{\cdot}3H_2O$. For both materials however, synthesis protocols reported in the literature for $Na_2Cu(CO_3)_2{\cdot}3H_2O$ and $K_2Cu(CO_3)_2$ lead to the presence of impurities. Synthesis have therefore been modified to obtain pure powder.

$K_2Cu(CO_3)_2$

A saturated solution of K_2CO_3 (99.0% Sigma Aldrich) is prepared, in which copper acetate (98% Sigma Aldrich) is added. After filtering the liquid part of this mix using Buchner filtration, the liquor is left to evaporate for a couple weeks. The colour evolution from light to intense dark blue is easily visible, and after the water is almost completely evaporated and the powder looks dry, it is laid on a filter paper to absorb the residual liquid, dragging the excess of K_2CO_3. Synthesis process is summarized on figure S1.

$Na_2Cu(CO_3)_2{\cdot}3H_2O$

The synthesis of the Na containing compound has been also described in the aforementioned literature[24,25,27,30]. However, its synthesis is slightly different from the previous K containing compound, since it is a two-step synthesis passing by an intermediate hydrated phase $Na_2Cu(CO_3)_2{\cdot}3H_2O$ [25]. The reaction principles are the same as in the case of K containing compound, aiming at reacting alkaline carbonate with copper acetate. However, in this case, synthesis leads to the formation of the tri-hydrated chalconatronite: $Na_2Cu(CO_3)_2{\cdot}3H_2O$. A solution of copper acetate is added to a saturated solution of Na_2CO_3 (99.5% Sigma Aldrich), without steering. After few hours, homogenization of the solution occurs, and it turns to a deep blue colour. After a week at room temperature, the solution becomes lighter and contains solid part. A Buchner system is used to filtrate the solution. The solid part is retained, and further water removed using filter paper. After 24h on the filter, small crystals of few hundred microns are obtained (see figure S2).

In this synthesis process, the solid part is used to obtain the final $Na_2Cu(CO_3)_2{\cdot}3H_2O$ crystals. However, the liquid part can be reused to perform new synthesis, just by adding copper acetate solution and do the same cycle again. In this process, the synthesis takes some time too, and here also, the quantities can be large. Indeed, more than 5 g of powder have been obtained in a single batch, and this does not represent a maximum and could be increased.

Dense ceramics were prepared with Spark plasma sintering (Dr. Sinter Lab spark plasma sintering system, Model SPS-511S/SPS-515S) in WC:Co 10 mm die using 0.3 g of powder for each sintering attempt. Tantalum foils were used to separate the sample from the die. Thermocouple is used to monitor temperature, in contact with the inner part of the die. A 12 ON/2 OFF pulse sequence is applied for all samples. Densification was continuously monitored by the displacement of a punch rod. A 30 °C/min heating ramp was used for all different sintering experiments, while temperature was varied from 300 °C to 350 °C for KCCO and from 200 to 300 °C for hyd-NaCCO. Pressure was set to 600 MPa and dwell time to 10 min for all samples. Sintering attempts were performed under primary vacuum of about 10 Pa. Powder and ceramic diffraction were performed with a Phillips X'Pert MPD X-ray diffractometer with the Bragg–Brentano geometry using Cu Kα1/Kα2 radiation ($10° < 2\theta < 80°$ range, step of 0.017°). The ceramics' relative densities were evaluated by geometrical measurements considering a theoretical density of 2.80 and 3.01 g/cm^3 for KCCO [31] and NaCCO [29] respectively. The ceramics' microstructures were observed on fracture surfaces, with a scanning electron microscope (JEOL 840 SEM). TGA measurements were performed with a Setaram tag2400 apparatus. Magnetic measurements were performed with a MPMS-7-XL (S.Q.U.I.D) magnetometer (Quantum Design) on ceramics. Zero-field cooled and field cooled data were collected with an applied field of 1 kOe and with increasing temperature from 2K to 300K. Silver electrodes were deposited on both surfaces of the ceramics and silver wires were subsequently used for sake of electrical connection. Once prepared for dielectric measurements, the ceramics were placed in a Quantum Design Physical Properties Measurement System (PPMS) from which a 9 T magnetic field can be applied. The dielectric measurements were carried out in the frequency range of $10^2 – 10^6$ kHz (the amplitude of the applied ac electric field being 1V) using an HP4194a impedance bridge, at heating and cooling rates between 0,2 and 1 K/min. Capacitance and dielectric losses measurements were first performed by scanning temperature with and without application of a magnetic field of 9T. In a second step, the magnetic field was swept from -0.6T to 0.6T for NaCCO and from -4 to 4 T for KCCO at 2K to evaluate the magnetoelectric behaviour of the samples.

Results and discussion

Following the development of quantitative synthesis protocols valid at the gram scale, the crystal structure of the precursor powders were investigated. Powders characterization were performed through XRD profile refinement (figure 1a and c) of synthesized powders. The resulting lattice parameters are summarized in table 1 and compared to literature data. Both powders exhibit the expected crystal structure (*i.e. Fdd2* space group for $K_2Cu(CO_3)_2$ and $P2_1/n$ for $Na_2Cu(CO_3)_2{\cdot}3H_2O$), with no evidence of secondary phases, along with a good match

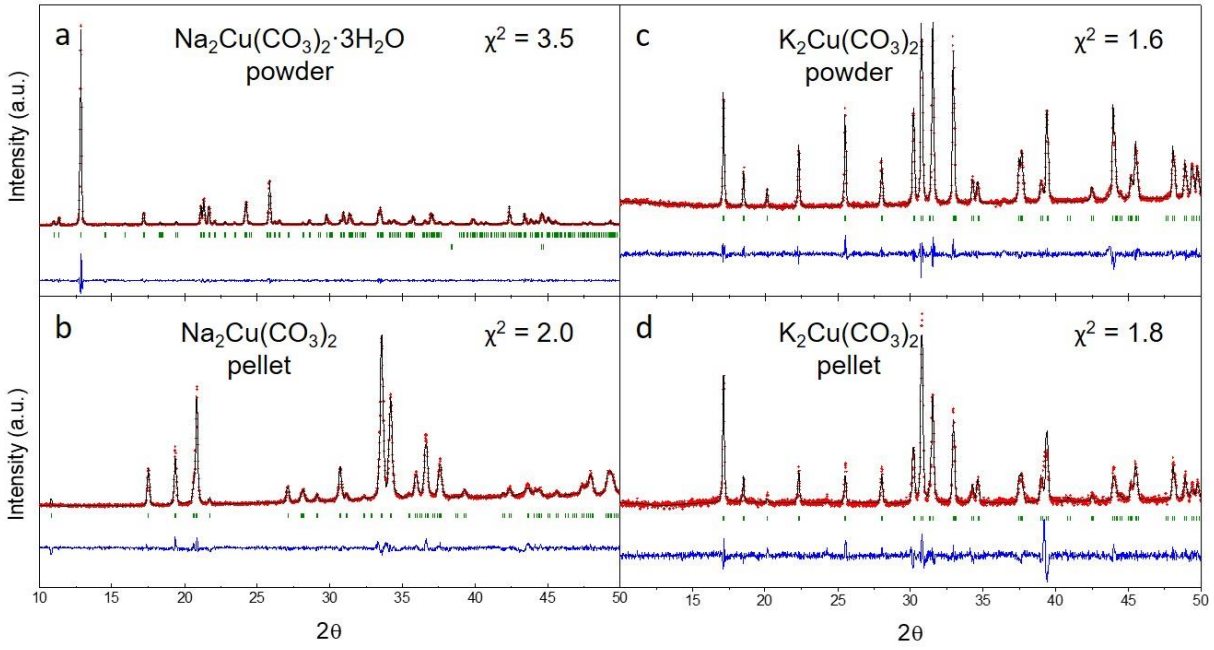

Figure 1: Profile XRD refinements of a) $Na_2Cu(CO_3)_2·3H_2O$ powder, b) $Na_2Cu(CO_3)_2$ ceramic sintered at 300 °C, c) $K_2Cu(CO_3)_2$ powder and d) $K_2Cu(CO_3)_2$ ceramic sintered at 350 °C. Red dots correspond to measured data, black line are simulated profile, blue are difference between black and red, and green marks represent Bragg positions for both phases.

between experimental and literature lattice parameters. The maximum deviation from literature data are limited to 0.09% for Hyd-NaCCO and 0.03% for KCCO. XRD analyses confirm the high crystalline purity of the synthesized powders.

Figure 2a and d display TGA performed respectively on hyd-NaCCO powder and KCCO powder. The trihydrated powder hyd-NaCCO shows three mass losses. The first one occurs in a double step loss from 55 to 80 °C with a mass loss of 2.2%, which must correspond to adsorbed water on the sample. This is expected since water is removed from the sample by drying at room temperature in air on a filter paper, so residual surface water is likely to be present. The second loss is the biggest loss, associated to 19% loss from 120 to 155 °C. This loss corresponds to the 3 H_2O molecules chemically linked to the carbonate (following dehydration equation 1), representing 19.7 wt.% theoretical mass loss.

$$Na_2Cu(CO_3)_2·3H_2O_{(s)} \rightarrow Na_2Cu(CO_3)_{2(s)} + 3H_2O_{(g)} \quad (1)$$

Eventually, the last loss from 220 to 280 °C with 14% loss corresponds to the mass fraction of carbonate groups in hyd-NaCCO (theoretically 15.5 wt.%), thus the loss corresponds to the decomposition of the sample, following the reaction:

$$Na_2Cu(CO_3)_{2(s)} \rightarrow Na_2CO_{3(s)} + CuO_{(s)} + CO_{2(g)} \quad (2)$$

Therefore, it could be expected that anhydrous phase can be obtained after simple dehydration of the powder in air between 160 and 220 °C, avoiding its decomposition starting at higher temperature. Attempts were made in this regard, leading to mixed phases (see figure S3) and confirms the necessity to process through a liquid route to crystallize the anhydrous phase (such as described in ref [29]) to produce the anhydrous form, NaCCO. However, this method represents a huge limitation since the obtained crystals (blue crystals) necessitate manual separation from impurities (white crystals) to obtain it pure. To avoid this issue, the choice was thus made to investigate the use of the hydrated powders for Cool-SPS experiments. Figure 2d displays the TGA measurement of KCCO powder. Again, three mass losses are observed. The first peak, from 160 to 210 °C, corresponds to 5% of total mass.

Table 1: Refined lattice parameters of synthesized powders and ceramics; reference values are displayed for comparison and ùax deviation calculated as the difference between sample and reference

	a (Å)	b (Å)	c (Å)	β (°)	maximum deviation
Hyd-NaCCO powder	9.6933(1)	6.0953(1)	13.7895(1)	91.915(1)	0.09%
Hyd-NaCCO ref [31]	9.696(2)	6.101(2)	13.779(3)	91.83(2)	-
NaCCO-300°C ceramic	6.1739(1)	8.1779(2)	5.6482(1)	116.260(1)	0.15%
NaCCO-200°C ceramic	6.1728(1)	8.1778(3)	5.6478(1)	116.242(1)	0.15%
NaCCO ref [29]	6.18(2)	8.19(2)	5.64(2)	116.2(2)	
KCCO powder	11.4238(2)	17.6519(2)	6.1526(1)	90	0.03%
KCCO-350°C ceramic	11.4215(3)	17.6555(5)	6.1502(2)	90	0.06%
KCCO ref [32]	11.425(3)	17.658(4)	6.154(2)	90	

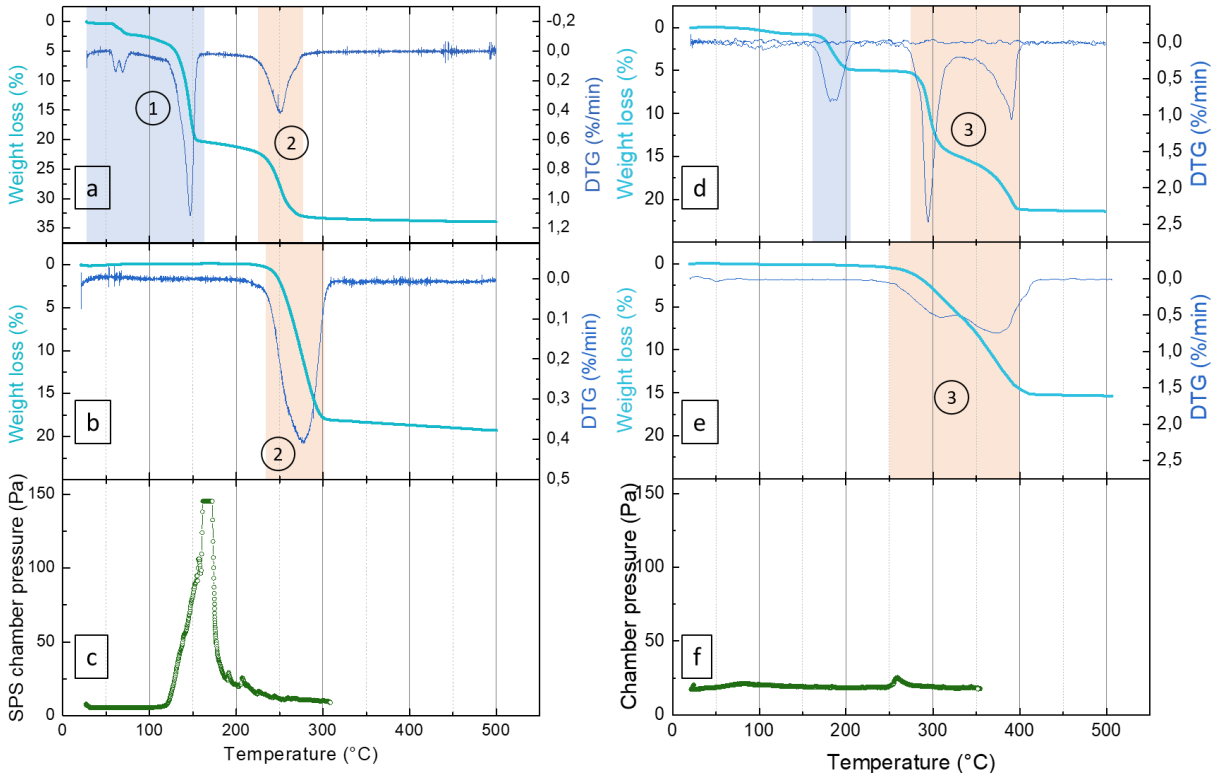

Figure 2: TGA measurement in air on a) $Na_2Cu(CO_3)_2{\cdot}3H_2O$ powder, b) $Na_2Cu(CO_3)_2$ ceramic sintered at 300°C d) $K_2Cu(CO_3)_2$ powder, e) $K_2Cu(CO_3)_2$ ceramic sintered at 350°C and SPS chamber pressure during sintering of c) $Na_2Cu(CO_3)_2{\cdot}3H_2O$ at 300 °C, 600 MPa and f) $K_2Cu(CO_3)_2$ at 350 °C, 600 MPa ; blue highlights represent dehydration steps while orange ones correspond to decomposition. Numbers on the figure relate to equation presented in the text.

According to the low temperature, this must correspond to adsorbed water which is expected to result from the synthesis protocol, as previously discussed for hyd-NaCCO. Then, two additional mass loss occur from 270 to 320 °C and 360 to 400 °C. They contribute to a total mass loss of 16.5 wt.%, which corresponds to the weight contribution from carbonate groups (theoretically 16.8 wt.%) release according to the following reaction:

$$K_2Cu(CO_3)_{2\,(s)} \rightarrow K_2CO_{3\,(s)} + CuO_{\,(s)} + CO_{2\,(g)} \qquad (3)$$

According to the TGA measurements made on powder (under air), we could determine that hyd-NaCCO dehydrates from 55 to 155 °C and decomposes above 160 °C, while KCCO dehydrates from 160 to 210 °C and further decomposes above 270 °C.

Both powders were manually crushed in an agate mortar and sintered by Cool-SPS. A uniaxial pressure of 600 MPa is applied on the samples all along the thermal cycle. Temperature is increased to 300 °C for hyd-NaCCO and 350 °C for KCCO at a heating rate of 30 °C/min, then it is maintained during 10 min and naturally cooled to room temperature.

Figure 1b and d display the XRD profile refinements of the corresponding ceramics. It is interesting to note the conversion of hyd-NaCCO into NaCCO after sintering, without any secondary phase. This suggests that reactivity of hyd-NaCCO is affected by the Cool-SPS environment (applied pressure, vacuum, current…). This is also of great interest since it shows a potential use for Cool-SPS as a tool to obtain pure phases that cannot be obtain through classical solid state treatments. In the present case, this allows us to avoid the precipitation of NaCCO from hyd-NaCCO through the liquid routes mentioned previously. In the case of KCCO, the phase is preserved upon sintering. This is further supported by table 1 showing the refined lattice parameters for both ceramics and compared to the literature data. They show a maximum deviation of 0.06% for KCCO and 0.15% for NaCCO with literature data. Therefore, they show a very good match with the expected phases. A sintering experiment was performed on hyd-NaCCO at 200 °C, confirming the total transition to the anhydrous phase, and its profile refinement leads to the same quality as the one obtained at 300 °C. This suggests us that anhydrous NaCCO can be obtained from 200 °C to 300 °C without formation of a secondary phase as observed in conventional heat treatment in furnace. This reinforces the interest of using Cool-SPS as a preparative and prospective tool.

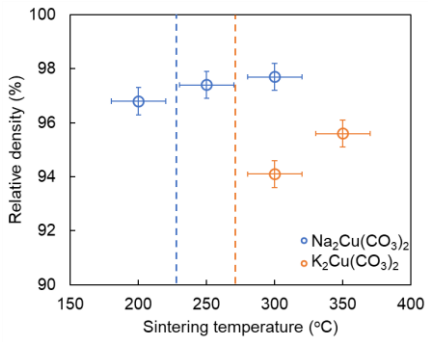

Figure 3: Densification of both powders for various temperature. Sintering pressure and time are set to 600 MPa and 10 min for each sample. Dotted lines represent the decomposition temperatures measured in TGA under air.

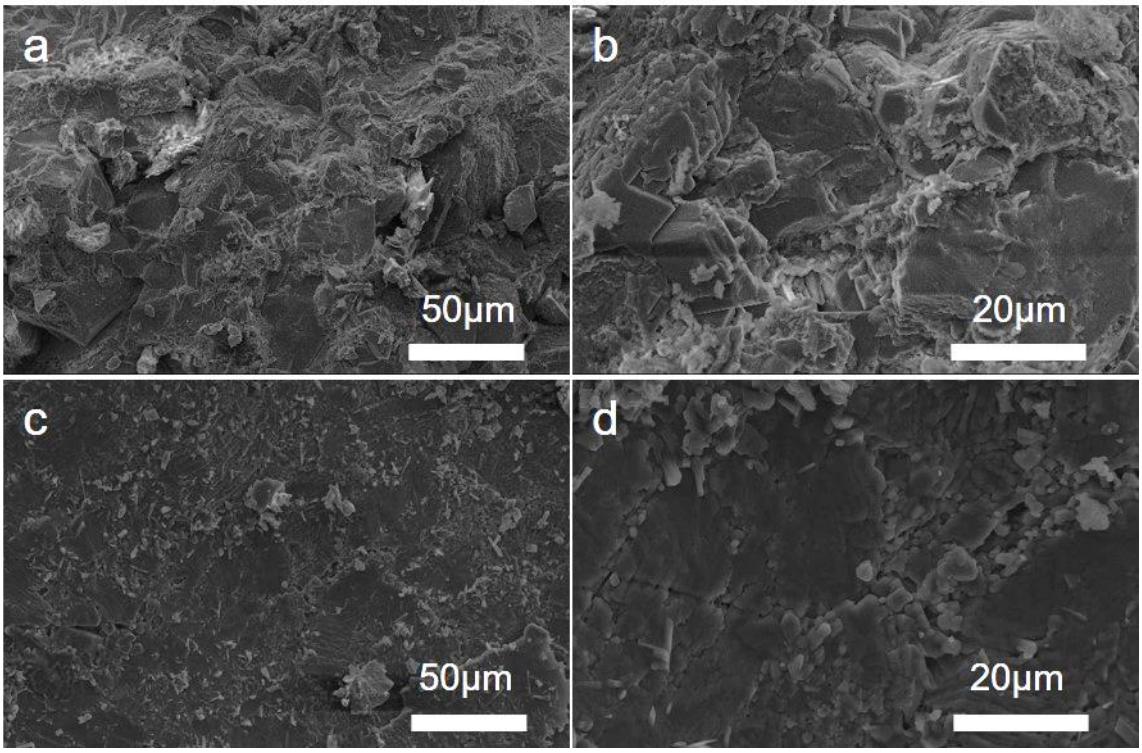

Figure 4: SEM observations of fractured ceramics of (a and b) $Na_2Cu(CO_3)_2$ sintered at 300 °C and (c and d) $K_2Cu(CO_3)_2$ sintered at 350 °C

Figure 2b and e display TGA measurements of the ceramics obtained by Cool-SPS. For NaCCO, a single mass loss is observed, which corresponds to 19% of NaCCO initial mass, and is associated the decomposition of the phase described in equation 2.

The absence of the two losses observed in the powders between 55-80 and 120-155 °C confirms that it corresponds to a H_2O loss of adsorbed and structural water respectively in the powder case. It also confirms that the sample after sintering totally dehydrates and the transition from hyd-NaCCO to NaCCO is complete. For KCCO, a single mass loss occurs as in the initial powder with a 16% weight loss, following equation 3. It is interesting to note that sintering temperatures used to obtain these ceramics are 70 °C above the decomposition temperature as measured in air after sintering. It further confirms the stabilization effect of the SPS environment for the present materials, confirming the previous observation made on other materials systems [3,12].

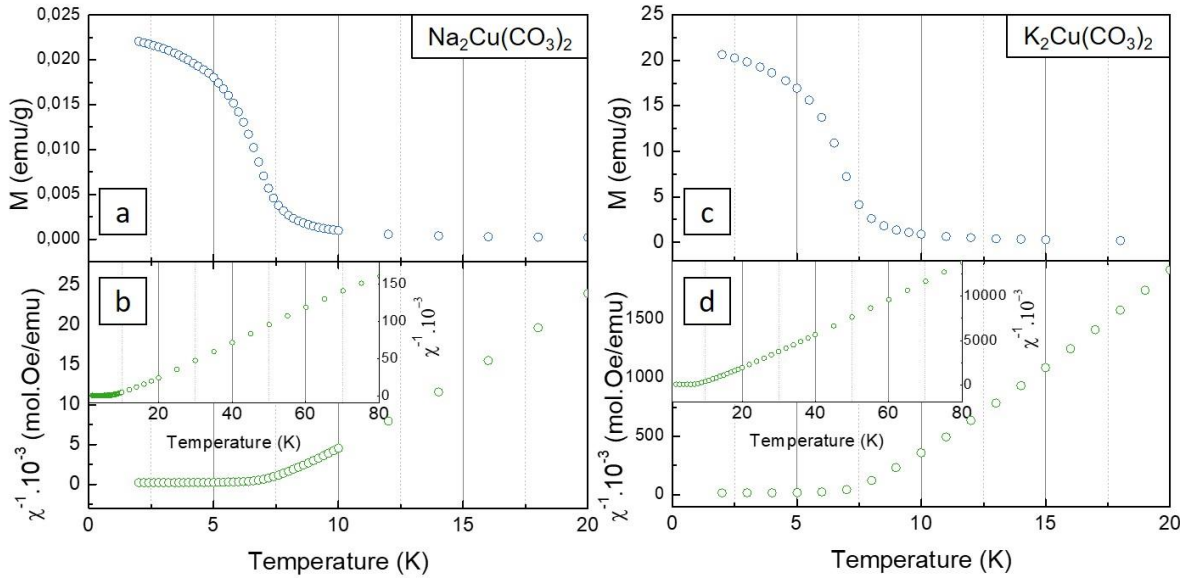

Figure 5: SQUID measurements on ceramics sintered at 300 °C for $Na_2Cu(CO_3)_2$ and 350 °C for $K_2Cu(CO_3)_2$. A-b) correspond to magnetization measurement, band d) correspond to inverse susceptibility measurement on the temperature range (0 – 20 K) with inset showing temperature range (0 – 80 K).

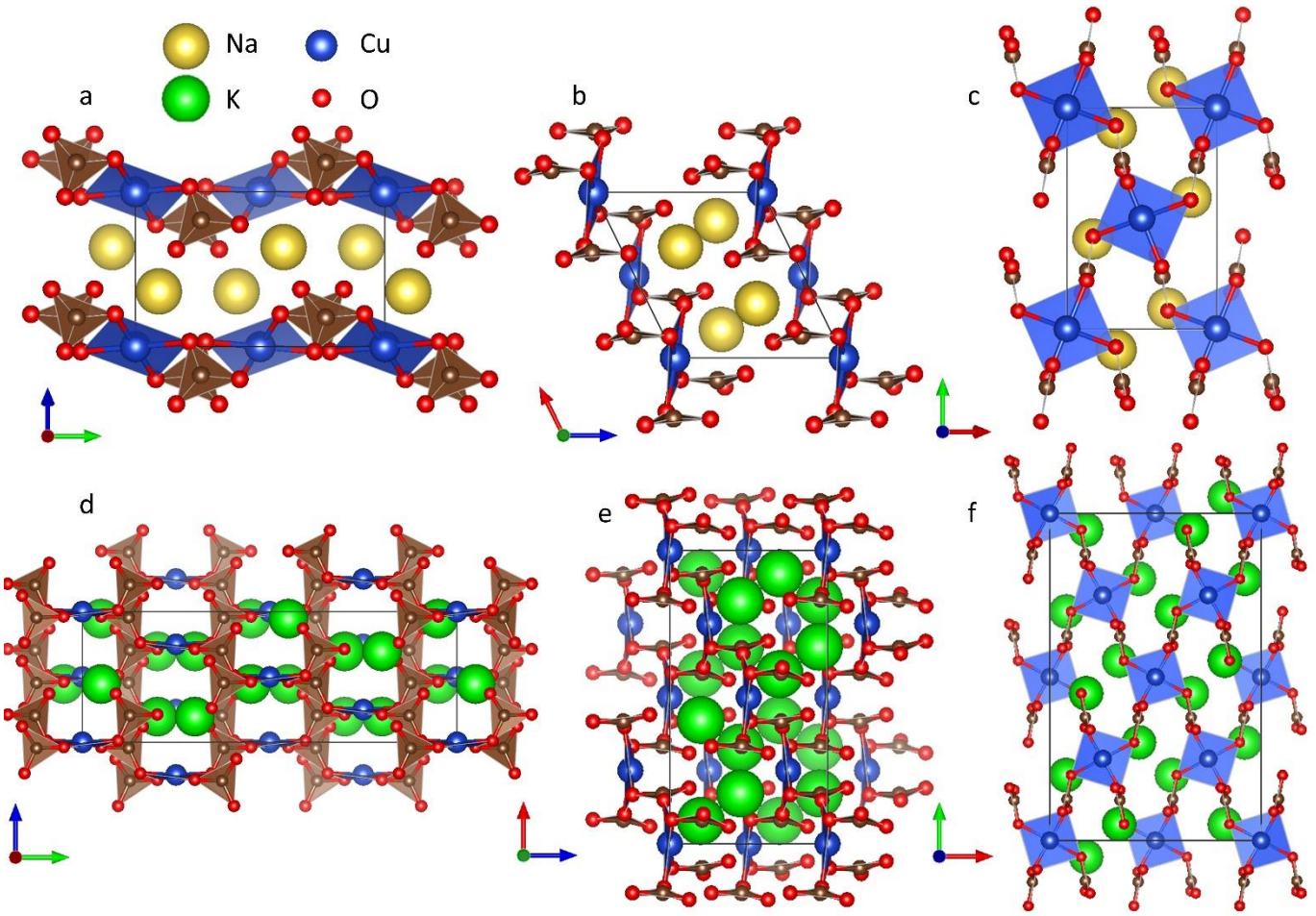

Figure 6: Crystal structure of (a-c) $Na_2Cu(CO_3)_2$ and (d-f) $K_2Cu(CO_3)_2$ in a, b and c axes; arrows correspond to crystal directions: red = a, green = b and blue = c.

Chamber pressure is recorded during sintering experiments and the data are presented on Figure 2c and d for hyd-NaCCO sintered at 300 °C and KCCO sintered at 350 °C respectively. For hyd-NaCCO, a pressure increase is observed from 120 to 200 °C, corresponding to the dehydration leading to NaCCO. Our experimental setup does not allow for pressure measurement above 145 Pa, which is the reason for the observation of a saturation at 145 Pa at the dehydration peak. Therefore, the maximum value of pressure cannot be determined. This water release is observed nearly in the same temperature range as dehydration during TGA measurement (55-155 °C). However, no further event is visible at higher temperature. This confirms that no decomposition occurs up to 300 °C in SPS, explaining the observation of a pure phase in XRD pattern of sintered samples. This also confirms the dehydration process during sintering. For KCCO, a small pressure increase up to 25 Pa appears from 250 to 270 °C. Thus, the origin of this small gas release is not yet deciphered, but may correspond to a slight dehydration of the powder. This is consistent with TGA performed on ceramic after sintering, showing no mass loss except the decomposition, pointing out the absence of water in the sample after sintering. Moreover, the absence of chamber pressure increase between 270 and 350 °C shows that KCCO is stable during SPS treatment, even 80 °C beyond its decomposition temperature measured in TGA.

Figure 3 shows density measurements for each ceramic. Decomposition temperatures are also displayed on the same figure as dotted lines. Densities range from 94.1 ± 0.5 to 95.6 ± 0.5% for KCCO sintered at temperatures from 250 to 350 °C and from 96.8 ± 0.5 to 96.7 ± 0.5% for NaCCO for samples sintered at temperatures from 200 °C to 300 °C. Cool-SPS processing allows for the stabilization of these two compounds 70 and 80 °C (NaCCO and KCCO respectively) above their decomposition temperature in air. Moreover, the decomposition limit in Cool-SPS environment has not been explored, therefore, the stabilization may be observed at temperatures above the one used in the present work.

The high density values measured geometrically on ceramics are confirmed by the microstructures observed in SEM (see figure 4). For both carbonate materials, grains over few tens of microns are observed, which may result from the synthesis method: single crystals were present in the powders that were crushed for sintering experiments. This suggests that even though large grains are present in the raw powder, sintering mechanism is efficient and high density ceramics can be obtained from large particles. One can assume that further adjustments of the powders particle size would lead to even

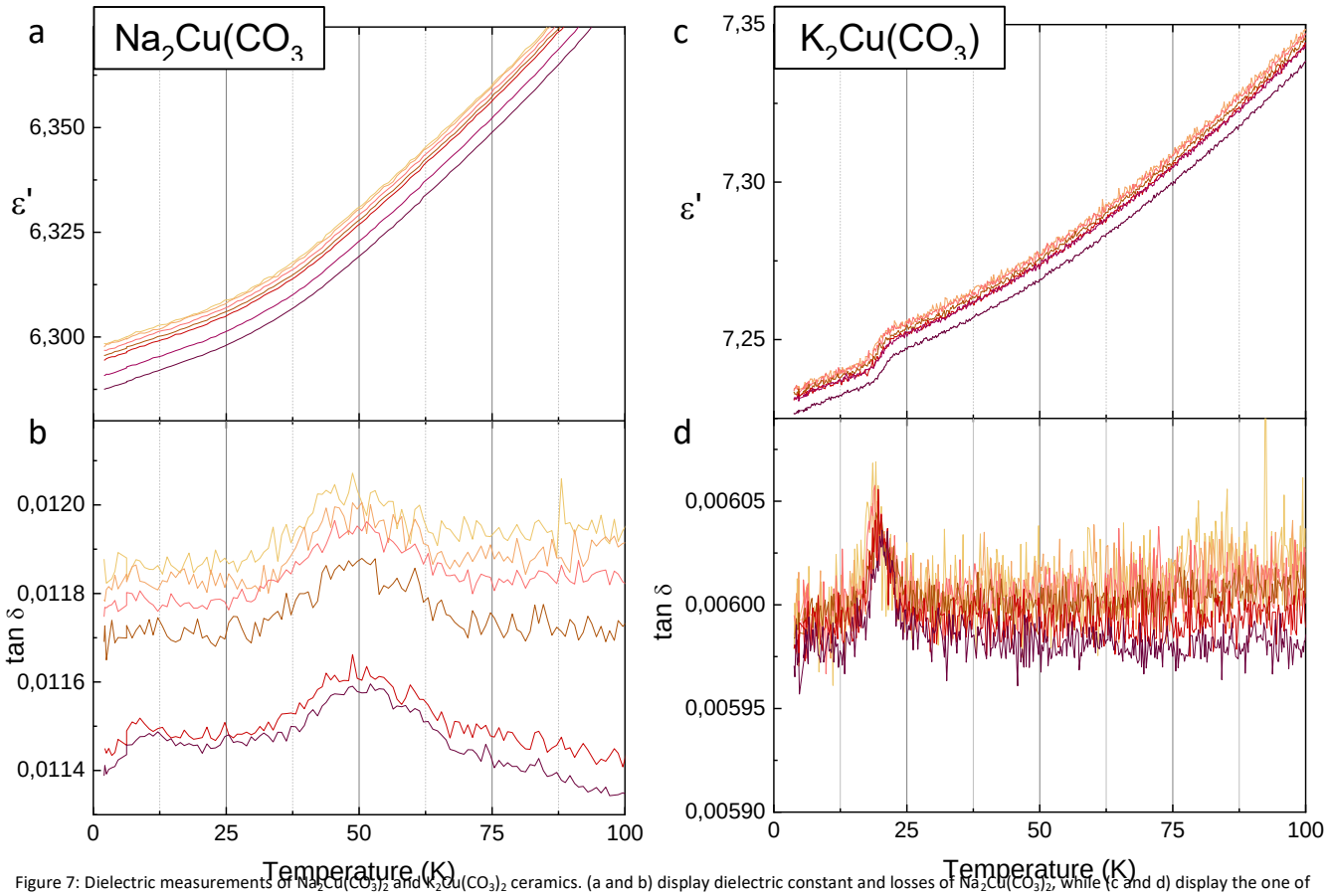

Figure 7: Dielectric measurements of $Na_2Cu(CO_3)_2$ and $K_2Cu(CO_3)_2$ ceramics. (a and b) display dielectric constant and losses of $Na_2Cu(CO_3)_2$, while (c and d) display the one of $K_2Cu(CO_3)_2$. Arrows represent frequency increase from 15 to 500 kHz

more dense samples, which is beyond the scope of the present work.

Magnetic characterizations are available in literature for both compositions [23,29,33], which are, in addition to XRD, a good way of probing chemical and crystalline quality. On the contrary, dielectric data are missing. Magnetic measurements on ceramics are displayed on figure 5 and show ZFC measurements from 2 to 80 K. Measurements show paramagnetic behaviour at high temperatures. Curie-Weiss fit give Weiss temperatures θ = 6.45 K for KCCO and θ = 8.93 K for NaCCO. These values are slightly lower than the one found in literature (respectively 9.7 K and 9.2 K for KCCO and NaCCO [22,23]) confirm the presence of ferromagnetic interactions in both compounds.

Both structures exhibit a different magnetization, resulting from different structure and magnetic couplings. Whereas KCCO has a 3D network (see Figure 6(d-f)), NaCCO has a layered structure made of Cu atoms in square sites delimited by carbonate groups lying in the ab plane (see Figure 6(a-c)). It should be noted that NaCCO is known as a ferromagnet exhibiting interlayer ferromagnetic interaction and intra-layer antiferromagnetic interactions [33]. However, a spin-flop transition is observed for these antiferromagnetic interactions for low fields (< 0.1 T), which has been determined on single crystal data [23]. Here the magnetic field applied during the measurement was larger than that triggering the spin-flop transition, and thus a ferromagnetic behaviour is observed. Curie constants were determined as C = 6.45×10^{-6} emu.K.mol^{-1} for KCCO and C = 4.36×10^{-4} emu.K.mol^{-1} for NaCCO. Considering the high density of the sintered samples, electrical characterizations can be performed with the assumption that porosity-related extrinsic contributions to dielectric response can be neglected.

Figure 6 displays dielectric permittivity and losses versus temperature from 2 to 100 K at various frequencies ranging from 50 to 500 kHz. On the one hand, NaCCO shows a monotonous decrease of both permittivity and losses on cooling, with only a change of slope in the range 25-50 K for the permittivity. The low level of losses confirms the high quality of the ceramic and points out the absence of significant dielectric anomaly in the explored temperature range. On the other, the dielectric behaviour of KCCO shows a step-like anomaly in permittivity and a peak in losses at 20 K. This dielectric anomaly is very similar to the one observed in other multiferroic systems like *R*Mn2O5 (*R* = Tb, Dy, Ho) [34]. However, in the present case, the dielectric anomaly nature is hard to determine due to the small amplitude of the phenomenon that prevented its probing by other experimental means (pyroelectric measurements were not successful to determine its nature). However, in that case too, the low level of dielectric losses confirms the high quality of the ceramics obtained by Cool-SPS (due to the absence of space charges associated to large porosity).

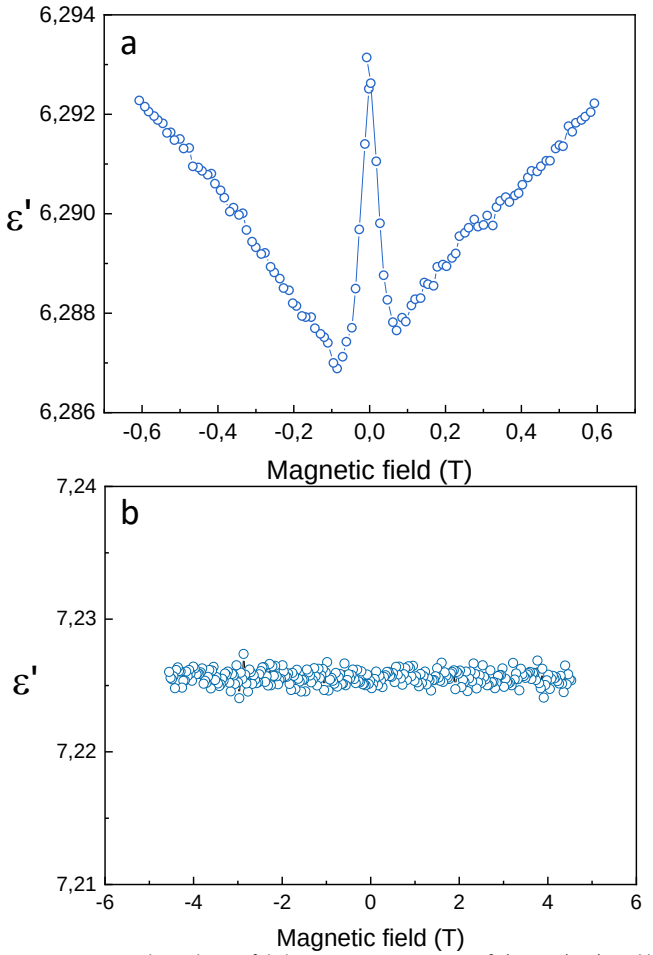

Figure 7: Magnetic dependence of dielectric permittivity at 2 K of a) $Na_2Cu(CO_3)_2$ and b) $K_2Cu(CO_3)_2$ ceramics respectively sintered at 300 °C and 350 °C

Figure 7 shows dependence of permittivity versus magnetic field at 2 K for NaCCO and KCCO. In the case of KCCO (Figure 7b), no evolution of dielectric permittivity is observed from -4 to 4 T. In contrast, NaCCO shows a permittivity decrease from 6,293 to 6,288 from 0 to 0.1 T, followed by a constant increase up to 0.6 T, restoring the zero field permittivity at 0.6T. This behaviour is essentially symmetric when opposite magnetic field is applied. The evolution of dielectric permittivity when varying magnetic field at constant temperature supports the presence of a magnetoelectric coupling in $Na_2Cu(CO_3)_2$. Moreover, the presence of an inversion at 0.1 T can be related to the presence of a spin-flop transition from an antiferromagnetic to a ferromagnetic state, as previously described by Gregson and Healy [33].

Conclusions

Both $Na_2Cu(CO_3)_2{\cdot}3H_2O$ and $K_2Cu(CO_3)_2$ powders were prepared through liquid route process with high purity at the gram scale. Using these powders for sintering, it was possible to densify them in the anhydrous form above 95% of their theoretical densities, by Cool-SPS processing at temperatures below 300 °C and 350 °C respectively. Not only this allowed to obtain high density, but it was also possible to achieve *in situ* dehydration of $Na_2Cu(CO_3)_2{\cdot}3H_2O$, leading to a phase pure dense ceramic of the anhydrous phase $Na_2Cu(CO_3)_2$. This offers a way of synthesizing this material in bulk quantities, which was impossible with previously reported methods, relying on manual sorting of single-crystals. After confirming phase purity using X-ray diffraction, SEM analysis confirmed the absence of visible porosity on fractured samples, demonstrating the efficiency of Cool-SPS for these two materials. Magnetic properties were measured on densified samples, confirming the magnetic behaviour reported in the literature, including the spin-flop transition in $Na_2Cu(CO_3)_2$. While the low level of dielectric losses confirmed the quality of the ceramic, a dielectric anomaly, warranting further investigation, has been highlighted in $K_2Cu(CO_3)_2$, which can be considered a candidate multiferroic. Eventually, magnetodielectric measurements were performed on both samples at 2 K, revealing $Na_2Cu(CO_3)_2$ as a candidate magnetoelectric materials. Fragile ferroics are thus a class of materials worthy of further investigations that are enabled by the efficiency of Cool-SPS for their preparation, including reactive routes, in ceramic form.

Conflicts of interest

There are no conflicts to declare.

References

[1] G. Goglio, A. Ndayishimiye, A. Largeteau, C. Elissalde, Scr. Mater. 158 (2019) 146–152.
[2] J. Guo, R. Floyd, S. Lowum, J.-P. Maria, T. Herisson De Beauvoir, J.H. Seo, C.A. Randall, Annu. Rev. Mater. Res. 49 (2019) 275–95.
[3] T. Herisson de Beauvoir, A. Sangregorio, I. Cornu, C. Elissalde, M. Josse, J. Mater. Chem. C 6(9) (2018) 2229–2233.
[4] A. Ndayishimiye, S. Buffière, M.A. Dourges, A. Largeteau, M. Prakasam, S. Mornet, O. Kaman, J. Zdeněk, J. Hejtmánek, G. Goglio, Scr. Mater. 148 (2018) 15–19.
[5] H. Guo, T.J.M. Bayer, J. Guo, A. Baker, C.A. Randall, Scr. Mater. 136 (2017) 141–148.
[6] H. Nakaya, M. Iwasaki, T. Herisson de Beauvoir, C.A. Randall, J. Eur. Ceram. Soc. 39 (2019) 396–401.
[7] H. Kähäri, M. Teirikangas, J. Juuti, H. Jantunen, Ceram. Int. 42 (2016) 11442–11446.
[8] T. Herisson De Beauvoir, K. Tsuji, X. Zhao, J. Guo, C.A. Randall, Acta Mater. 186 (2020) 511–516.
[9] J. Guo, X. Zhao, T. Herisson De Beauvoir, J.H. Seo, S.S. Berbano, A.L. Baker, C. Azina, C.A. Randall, Adv. Funct. Mater. 28 (2018) 1801724.
[10] T. Herisson de Beauvoir, S. Dursun, L. Gao, C. Randall, ACS Appl. Electron. Mater. 1 (2019) 1198–1207.
[11] T. Herisson de Beauvoir, F. Molinari, U.C. Chung-Seu, D. Michau, D. Denux, M. Josse, J. Eur. Ceram. Soc. 38 (2018) 3867–3874.
[12] T. Herisson de Beauvoir, A. Sangregorio, A. Bertrand, C.

Payen, D. Michau, U.-C. Chung-Seu, M. Josse, Ceram. Int. 45 (2019) 9674–9678.
[13] S.H. Bang, T. Herisson de Beauvoir, C.A. Randall, J. Eur. Ceram. Soc. 39 (2019) 1230–1236.
[14] T. Herisson de Beauvoir, V. Villemot, M. Josse, Solid State Sci. 102 (2020) 106171.
[15] A. Ndayishimiye, M.Y. Sengul, S.H. Bang, K. Tsuji, K. Takashima, T. Hérisson de Beauvoir, D. Denux, J. Thibaud, A.C.T. van Duin, C. Elissalde, G. Goglio, C.A. Randall, J. Eur. Ceram. Soc. (2019).
[16] C. Manière, L. Durand, A. Weibel, C. Estournès, Acta Mater. 102 (2016) 169–175.
[17] M. Biesuz, G. Taveri, A.I. Duff, E. Olevsky, D. Zhu, C. Hu, S. Grasso, Adv. Appl. Ceram. 119 (2020) 75–89.
[18] S. Funahashi, J. Guo, H. Guo, K. Wang, A.L. Baker, K. Shiratsuyu, C.A. Randall, J. Am. Ceram. Soc. 100 (2017) 546–553.
[19] J. Guo, H. Guo, D.S.B. Heidary, S. Funahashi, C.A. Randall, J. Eur. Ceram. Soc. 37 (2016) 1529–1534.
[20] A. Ndayishimiye, A. Largeteau, M. Prakasam, S. Pechev, M.A. Dourges, G. Goglio, Scr. Mater. 145 (2018) 118–121.
[21] H. Guo, J. Guo, A. Baker, C.A. Randall, J. Am. Ceram. Soc. 100 (2017) 491–495.
[22] A.K. Gregson, N.T. Moxon, Inorg. Chem. 21 (1982) 3464–3466.
[23] A.K. Gregson, N.T. Moxon, Inorg. Chem. 20 (1981) 78–81.
[24] S.U. Pickering, J. Chem. Soc. Trans. 94 (1911) 800–811.
[25] M.P. Applebey, K.W. Lane, J. Chem. Soc. 113 (1918) 609–622.
[26] S.U. Pickering, Journalof Chem. Soc. Trans. 95 (1909) 1409–1429.
[27] Deville, Ann. Chim. Phys. (1856).
[28] P.S. Brotherton, A.H. White, J. Chem. Soc. Dalt. Trans. 21 (1973) 2338–2340.
[29] P.C. Healy, A.H. White, J. Chem. Soc. Dalt. Trans. (1972) 1913–1917.
[30] W.C. Reynolds, J. Chem. Soc. Trans. 73 (1898) 262–267.
[31] A. Mosset, J.J. Bonnet, J. Galy, Zeitschrift Für Krist. 148 (1978) 165–177.
[32] B.N. Figgis, P.A. Reynolds, A.H. White, G.A. Williams, J. Chem. Soc. Dalt. Trans. (1981) 371.
[33] A.K. Gregson, P.C. Healey, Inorg. Chem. 17 (1978) 2969–2970.
[34] C.R. Dela Cruz, F. Yen, B. Lorenz, S. Park, S.W. Cheong, M.M. Gospodinov, W. Ratcliff, J.W. Lynn, C.W. Chu, J. Appl. Phys. 99 (2006).